nature cell biology

Myosin IIIa boosts elongation of stereocilia by transporting espin 1 to the plus ends of actin filaments

Felipe T. Salles[1,6], Raymond C. Merritt, Jr[1,2,6], Uri Manor[1], Gerard W. Dougherty[1,5], Aurea D. Sousa[1], Judy E. Moore[3], Christopher M. Yengo[3], Andréa C. Dosé[4] and Bechara Kachar[1,7]

Two proteins implicated in inherited deafness, myosin IIIa[1], a plus-end-directed motor[2], and espin[3–6], an actin-bundling protein containing the actin-monomer-binding motif WH2, have been shown to influence the length of mechanosensory stereocilia[7,8]. Here we report that espin 1, an ankyrin repeat-containing isoform of espin[6], colocalizes with myosin IIIa at stereocilia tips and interacts with a unique conserved domain of myosin IIIa. We show that combined overexpression of these proteins causes greater elongation of stereocilia, compared with overexpression of either myosin IIIa alone or espin 1 alone. When these two proteins were co-expressed in the fibroblast-like COS-7 cell line they induced a tenfold elongation of filopodia. This extraordinary filopodia elongation results from the transport of espin 1 to the plus ends of F-actin by myosin IIIa and depends on espin 1 WH2 activity. This study provides the basis for understanding the role of myosin IIIa and espin 1 in regulating stereocilia length, and presents a physiological example where myosins can boost elongation of actin protrusions by transporting actin regulatory factors to the plus ends of actin filaments.

Stereocilia, the prominent actin protrusions on the apical surfaces of sensory hair cells, emerge early during development and their lengths are maintained at fixed heights for the lifetime of the organism. The bundle of parallel actin filaments that make up the core of each stereocilium is continually renewed, with the entire actin bundle constantly assembled at the tip, treadmilling downward and disassembling at the base[9–11]. Given that stereocilia can be up to 100 μm in length, it is likely that some form of regulated transport is necessary to localize components of the actin polymerization machinery to the plus end of actin filaments. Although several myosins have been shown to alter stereocilia length and shape, depending on their expression levels[9,12–16], the mechanisms by which these motors or their binding partners regulate actin dynamics and stereocilia length remain unclear.

Using antibodies specific for the ankyrin repeat domain (ARD) of espin 1 (Supplementary Information, Fig. S1), we show localization at stereocilia tips with a tip-to-base gradient distribution (Fig. 1) similar to that previously described for myosin IIIa. Immunofluorescence of espin 1 was more intense in the longer stereocilia where the characteristic tip-to-base fluorescence intensity gradient also had a longer decay length (Fig. 1g, h). In contrast to other espin isoforms, which are present inside the actin core and along the entire stereocilia length[8], espin 1 was excluded from the actin cores and formed a thimble-like distribution at the tips of stereocilia (Fig. 1). Immunofluorescence in developing hair cells of the rat organ of Corti showed that espin 1 can be detected at the tips of stereocilia during their elongation and maturation phases (Fig. 1k–m). To confirm the localization of espin 1 at the tips of stereocilia, we overexpressed GFP–espin 1 in organotypic cultures of hair cells. Transfected hair cells show that GFP–espin 1 localizes at the tips of stereocilia, showing a tip-to-base gradient of intensity (Fig. 2) comparable to the immunolocalization (Fig. 1). These localization patterns — tip-to-base gradients and thimble-like distributions[7], as well as the temporal expression pattern[17] — closely match those of myosin IIIa. We hypothesized that targeting espin 1 to stereocilia tips, which is the site of actin polymerization[9,11], influences actin polymerization and stereocilia elongation. Analysis of the heights of stereocilia of cochlear and vestibular hair cells transfected with GFP–espin 1 showed that stereocilia were elongated when espin 1 was overexpressed (Fig. 2), consistent with our hypothesis.

The striking similarity of the tip-to-base gradient localization of both espin 1 and myosin IIIa prompted us to investigate whether myosin IIIa helps localize espin 1 to the tips of stereocilia and whether they have a combined role in the regulation of stereocilia length. We compared stereocilia length in hair cells transfected with espin alone, myosin IIIa alone and with a combination of both plasmids (Fig. 2). Hair cells transfected with myosin IIIa and espin 1 showed an increase in stereocilia length, higher than the combined increase observed for myosin IIIa alone and espin 1 alone (Fig. 2). It is important to note that any analysis of lengthening due to overexpression of myosin IIIa and espin 1 in hair cells must take into

[1]Laboratory of Cell Structure and Dynamics, National Institute on Deafness and Other Communication Disorders, National Institutes of Health, Bethesda, MD 20892, USA. [2]Department of Biology, University of Maryland, College Park, MD 20742, USA. [3]Department of Biology, University of North Carolina at Charlotte, Charlotte, NC 28223, USA. [4]Department of Molecular and Cell Biology, University of California, Berkeley, CA 94720, USA. [5]Current address: Consorzio Mario Negri Sud, Department of Cell Biology and Oncology, Santa Maria Imbaro, Chieti, Italy 66030.
[6]These authors contributed equally to the work.
[7]Correspondence should be addressed to B.K (e-mail: kacharb@nidcd.nih.gov)

Received 13 November 2008; accepted 19 January 2009; published online 15 March 2009; DOI: 10.1038/ncb1851

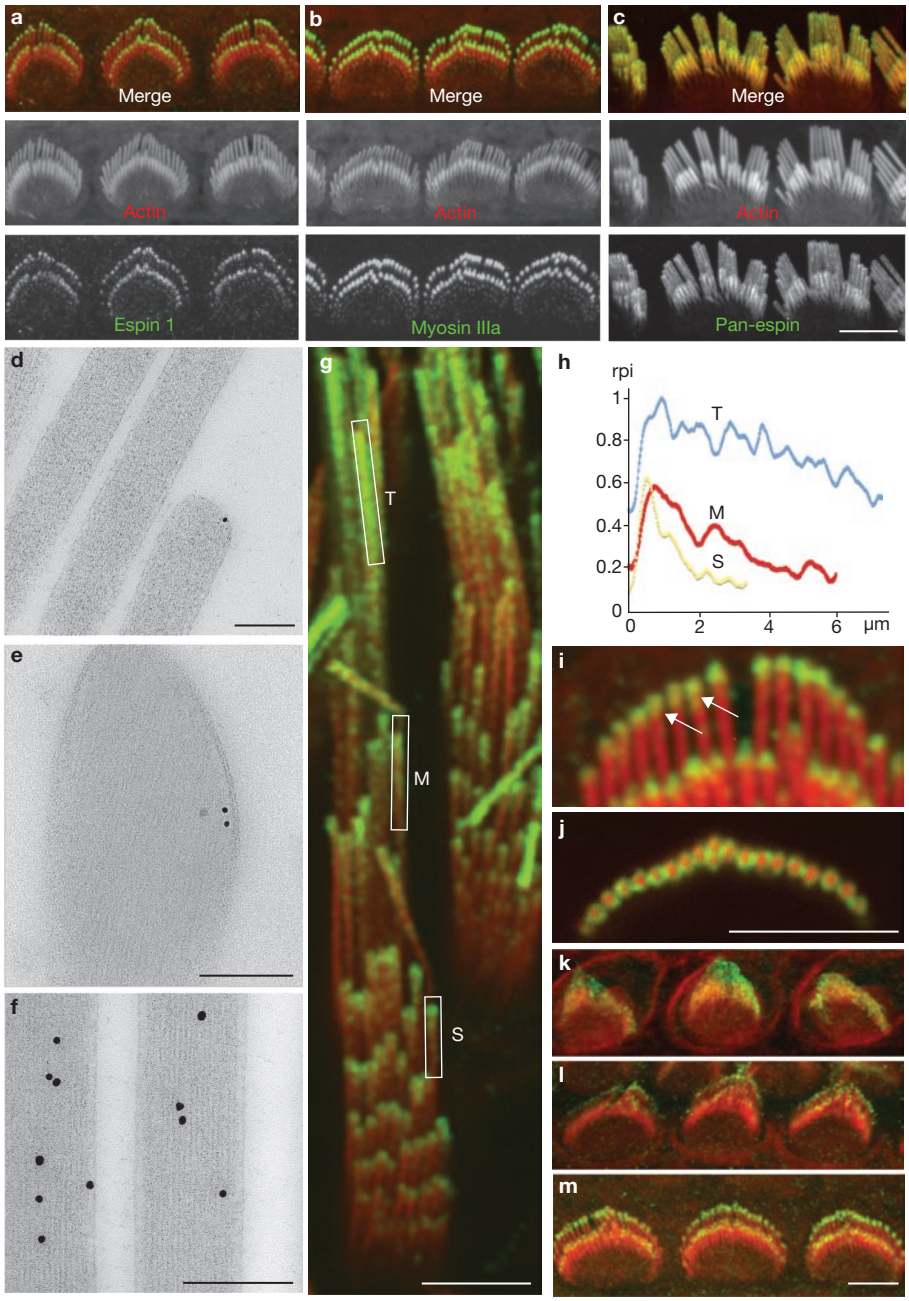

Figure 1 Espin 1 distribution in stereocilia is similar to myosin IIIa distribution. (**a**–**c**) Confocal images show that espin 1 (green, **a**) localized at the tips of stereocilia in rat cochlear hair cells at postnatal day (P) 6 matches the localization observed for myosin IIIa (green, **b**). In contrast, pan-espin labelling (green) is seen along the entire stereocilia (**c**). Scale bar, 5 μm. (**d**–**f**) Immunogold labelling shows espin 1 localized at the tip of stereocilia around the actin core (**d**, **e**), whereas labelling with a pan-espin antibody shows localization throughout the entire stereocilia actin cores (**f**) in plunge frozen vestibular (**d**, **f**) or directly frozen cochlear (**d**) tissues obtained from adult rats. Scale bars, 200 nm. (**g**) Espin 1 (green) localization in guinea pig vestibular stereocilia reveals a tip-to-base gradient that is more extended in longer stereocilia (inset T) than medium (inset M) and short (inset S) stereocilia. (**h**) Measurements of green (espin 1) and red (actin) relative pixel intensity (rpi) of fluorescence along the stereocilia for each rectangular inset in **g** confirm this tip-to-base concentration gradient of espin 1 immunofluorescence. (**i**, **j**) Longitudinal (**i**) and cross-section (**j**) images reveal a thimble-like distribution of espin 1 (green) at the tips of stereocilia in P8 rat cochlear hair cells. (**k**–**m**) Immunofluorescence of rat cochlear hair cells at different developmental time-points shows that espin 1 targets stereocilia tips as early as P0 (**k**) and undergoes progressive compartmentalization at the tips during P2 (**l**) and P4 (**m**), reaching a peak of intensity at about P6 as shown in **b**. Scale bars, 5 μm. Antibodies: espin 1 (PB539), myosin IIIa (PB638) and pan-espin (PB127). In all immunofluorescence images, the immunolabelling was visualized using Alexa-488-conjugated secondary antibody and F-actin (red) is visualized using Alexa 568-phalloidin.

account intrinsic limitations due to natural variations in stereocilia length and, importantly, the fact that stereocilia are already quite elongated and express substantial amounts of endogenous espin 1 and myosin IIIa.

We tested whether myosin IIIa can effectively interact with and transport espin 1 in COS-7 cells, using filopodia as a model to study actin protrusions. Myosin IIIa and espin 1 are not naturally expressed at detectable

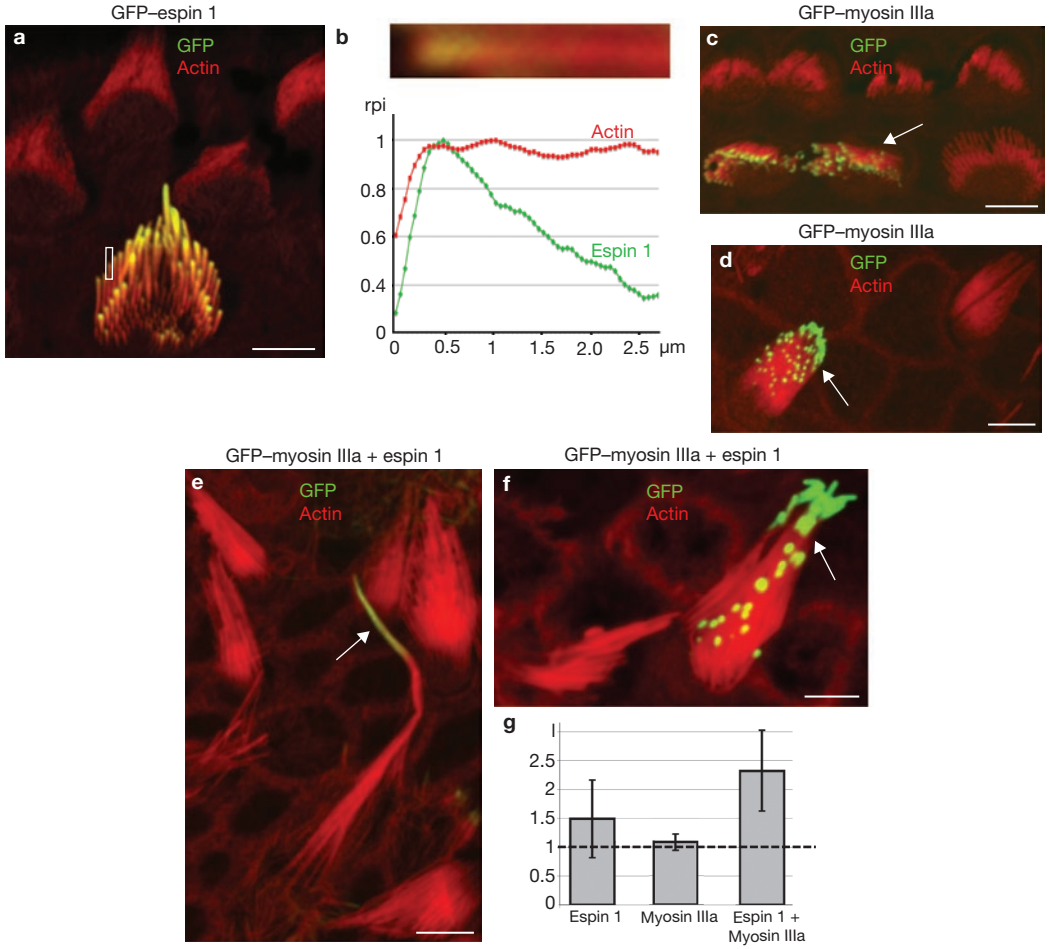

Figure 2 Espin 1 alone or when overexpressed with myosin IIIa elongates stereocilia. (**a**) GFP–espin 1 localizes to stereocilia tips in a tip-to-base gradient distribution in transfected cultured organ of Corti hair cells. (**b**) High magnification close-up view (upper panel) and measurement of the relative pixel intensity (rpi, lower panel) of GFP–espin 1 and actin (Alexa 568-phalloidin) fluorescence along the distal portion of the stereocilia shown in the rectangular inset in **a** matches the tip-to-base concentration-gradient observed for endogenous espin 1 (Fig. 1h). (**c**–**f**) Organ of Corti (**c**) and vestibular (**d**) hair cells transfected with GFP–myosin IIIa show tip localization similar to that of espin 1. Co-transfection of vestibular hair cells with GFP–myosin IIIa (arrow, green) and untagged espin 1 together (**e**, **f**, images of two different cells) produce longer stereocilia than in hair cells transfected with GFP–espin 1 alone (**a**) or with GFP–myosin IIIa alone (**c**, **d**). (**g**) The average ratios of stereocilia length (I) between transfected (H_T) and neighbouring non-transfected (H_{NT}) cells, $I = \frac{H_T}{H_{NT}}$. GFP–espin 1 alone = 1.5 ± 0.67, $n = 19$ (~50% increase); GFP–myosin IIIa alone = 1.1 ± 0.14, $n = 16$ (~10% increase); and GFP–myosin IIIa and espin 1 = 2.3 ± 0.69, $n = 14$, (~130% increase). Note that a value of I = 1 (indicated by the dotted line in the graph) corresponds to a zero percent increase in length. Data are mean ± s.d.; the mean value for the hair cells co-transfected with espin1 and myosin IIIa was significantly higher than that of the cells transfected with espin 1 alone ($P = 0.002$, ANOVA); the mean bundle heights for hair cells transfected with myosin IIIa alone were not significantly higher than the controls ($P = 0.149$, ANOVA). Scale bars, 5 μm.

levels in COS-7 cells[7]. Myosin IIIa has been shown to induce filopodial actin protrusions and localize to their tips in cultured cells particularly well when its kinase domain is removed (myosin IIIa$^{\Delta K}$)[7,18], suggesting that the kinase could serve to downregulate the functional activity of myosin IIIa. We examined the distribution of co-expressed mCherry–ARD of espin 1 with GFP-tagged myosin IIIa$^{\Delta K}$ (Fig. 3). We also co-expressed mCherry–ARD with GFP-tagged myosin X and GFP-tagged myosin XVa. As all of these myosins accumulate at the tips of filopodia[13,16,19], they provide a well-defined spatial compartment where any potential interaction can be clearly visualized. Co-transfections showed that mCherry–ARD is efficiently targeted to the tips of filopodia initiated by myosin IIIa$^{\Delta K}$, but not by myosins X or XVa (Fig. 3a), demonstrating a specific colocalization of ARD with myosin IIIa. Live imaging of COS-7 cells transfected with GFP–myosin IIIa$^{\Delta K}$ and mCherry–ARD showed dynamic colocalization at the filopodia tips from the early steps of their initiation and elongation (Fig. 3b; Supplementary Information, Movie 1). Live imaging also showed matching forward and rearward intra-filopodial movements of the GFP–myosin IIIa$^{\Delta K}$ and mCherry–ARD fluorescence puncta while maintaining steady-state tip-to-base distributions (Fig. 3c; Supplementary Information, Movies 2, 3), similar to the distributions of myosin IIIa and espin 1 observed in stereocilia (Figs 1, 2). The intensity profiles for mCherry–ARD and GFP–myosin IIIa$^{\Delta K}$ within each frame of the video (Fig. 3c) are closely correlated (cross-correlation = ~0.990), supporting the view that these two proteins traffic together in the filopodia. The interaction between espin 1 ARD and myosin IIIa$^{\Delta K}$ was confirmed with a GST pulldown assay (Fig. 3e). The dynamic localization of espin 1 ARD at filopodia tips when co-transfected with myosin IIIa, but not with myosin X or with myosin XVa, along with our GST pulldown assay results, led us to hypothesize that myosin IIIa transports espin 1 to the tips of stereocilia.

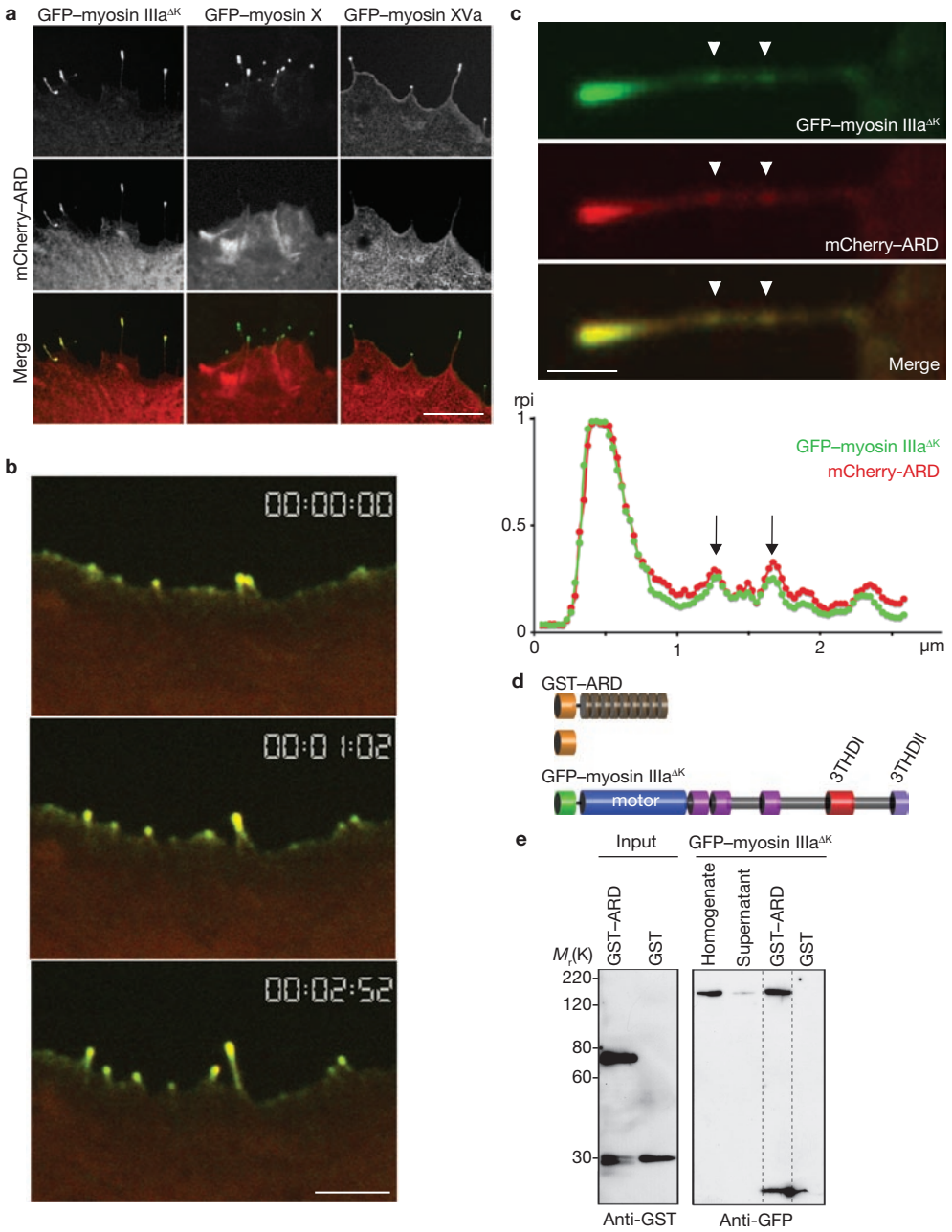

Figure 3 Espin 1 interacts with myosin IIIa through its ankyrin repeats domain (ARD) in transfected COS-7 cells. (**a**) mCherry-tagged espin 1 ARD shows filopodia tip localization when co-transfected with GFP–myoIIIa$^{\Delta K}$ but failed to localize at the filopodia tips when co-transfected with GFP–myosin X or GFP–myosin XVa. Scale bar, 5 μm. (**b**) Selected video images from a time-lapse video (Supplementary Information, Movie 1) show co-transport of GFP–myoIIIa$^{\Delta K}$ and mCherry–ARD during the formation and extension of filopodia in COS-7 cells. Scale bar, 2.5 μm. (**c**) Single representative frame from a time-lapse video of a single filopodium (Supplementary Information, Movie 2) graph with the normalized relative pixel intensity of the fluorescence along the filopodium show co-distribution (cross-correlation of the green and red intensity values = 0.990 for this frame; the average cross-correlation for six randomly selected frames from the same video was 0.99) of GFP–myoIIIa$^{\Delta K}$ and mCherry–ARD forming a tip-to-base gradient and colocalization of the green and red fluorescence puncta (arrowheads) corresponding to the co-transport of GFP–myoIIIa$^{\Delta K}$ and mCherry–ARD trafficking into and out of the tip of the filopodia. Scale bar, 0.5 μm. **(d)** Schematic representation of the constructs analysed in this figure. GST, glutathione S-transferase; GFP, green fluorescence protein; myosin IIIa$^{\Delta K}$, myosin IIIa with a deletion of it kinase domain; 3THDI and 3THDII, myosin IIIa tail homology domains 1 and 2, respectively. (**e**) Western blots of GST pulldowns show that purified GST–ARD co-precipitates with GFP–myosin IIIa$^{\Delta K}$, but not with GST alone. Precipitates were detected using anti-GST and anti-GFP antibodies.

We next asked which specific region of myosin IIIa is involved in the interaction with espin 1. Myosin IIIa has two conserved tail homology domains, designated as 3THDI and 3THDII[20]. We first co-transfected COS-7 cells with espin 1 and GFP–myosin IIIa and showed that the two proteins colocalize at actin bundles as well as at filopodia tips (Fig. 4a, b). This pattern of colocalization was abolished when we used a GFP–myosin IIIa construct that lacks the portion of the tail containing both 3THDI and 3THDII (GFP–myoIIIa$^{\Delta 32}$; Fig. 4a, b; Supplementary Information,

Table S1, Fig. S2). We next co-transfected COS-7 cells with espin 1 and with a GFP-tagged tail portion lacking 3THDII (GFP–tail$^{\Delta 3THDII}$; Fig. 4a, b) and narrowed down the region of interaction to the 3THDI and its immediate flanking regions. We observed colocalization of espin 1 with GFP–myosin IIIa tail that contained only the 3THDI domain (GFP–3THDI; Fig. 4a, b), but not with regions of only the myosin IIIa tail immediately amino-terminal (pre3THDI) or carboxy-terminal (post3THDI) to the 3THDI domain (Fig. 4a, b). This suggests that the 3THDI domain is necessary for the myosin IIIa–espin 1 interaction. Together these data suggest that espin 1 and myosin IIIa interact specifically through their ARD and 3THDI domains, respectively. We verified this interaction *in vitro* using a GST pulldown assay and showed that GST–ARD binds to GFP–3THDI, but not to the pre3THDI or post-3THDI regions (Fig. 4c).

The fact that stereocilia length can be influenced by either espin 1 (refs 3, 8) or myosin IIIa[7], along with the observation that they both localize to the same compartment at stereocilia tips and interact biochemically, suggests a combined functional role for the myosin IIIa–espin 1 complex in the elongation of stereocilia F-actin. We discovered that COS-7 cells co-transfected with myosin IIIa$^{\Delta K}$ and espin 1 (Fig. 5a–c) show filopodial actin protrusions that can be up to ten times longer (mean length = 14.3 ± 9.1 μm; number of cells, n_c = 18; number of filopodia, n_f = 56) than those transfected with myosin IIIa$^{\Delta K}$ alone (1.7 ± 0.83 μm, n_c = 12, n_f = 49), or with espin 1 alone (1.3 ± 0.28 μm, n_c = 13, n_f = 104). Mean lengths of filopodia of COS-7 cells transfected with an empty GFP vector was 1.26 ± 0.7 (n_c = 10, n_f = 59). The synergistic effect between myosin IIIa and espin 1 is specific for myosin IIIa, as elongation was not enhanced when espin 1 was co-expressed with either myosin X (2.40 ± 1.50 μm, n_c = 16, n_f = 165) or myosin XVa (2.08 ± 1.63 μm, n_c = 15, n_f = 134).

We used myosin IIIa without the kinase domain to observe the behaviour of the dephosphorylated and more functionally active myosin. To exclude the possibility that deletion of the kinase domain produces aberrant behaviour, we developed a kinase-dead construct, myosin IIIa^{K50R} (Supplementary Information, Table S1). This construct allowed us to examine the role of autophosphorylation in the regulation of motor function, which in turn enabled us to investigate the role of myosin IIIa motor function in espin 1 tip-localization activity. We have determined that inactivation of the myosin IIIa kinase in a myosin IIIa 2IQ construct reduces K_{ATPase}, yet it does not affect maximal ATPase activity (Supplementary Information, Table S2 and Fig. S3). We next evaluated the role of kinase activity in myosin IIIa tip localization in COS-7 cells using GFP-tagged constructs. Full-length myosin IIIa^{K50R} localized more efficiently to the tips of filopodia in COS-7 cells (39% at tips n_c = 137) than wild-type (5% at tips n_c = 200), although not as strikingly as myosin IIIa$^{\Delta K}$ (93% at tips n = 105). Furthermore, co-expression of myosin IIIa^{K50R} and espin 1 (Fig. 5e) produced longer filopodia (mean length = 5.93 ± 3.10 μm, n_c = 15, n_f = 89) than those produced by co-expression of wild-type myosin IIIa and espin 1 (3.7 ± 3.2 μm, n_c = 15, n_f = 63; Fig. 5d), but not as long as those seen with myosin IIIa$^{\Delta K}$ and espin 1 co-expression. These data show that myosin IIIa motor ATPase activity parallels the ability of myosin IIIa to localize to filopodia tips and to elongate filopodia when co-expressed with espin 1.

Interestingly, espin 1 co-expressed with a myosin IIIa$^{\Delta K}$ lacking the tail domain downstream of exon 32 (myosin IIIa$^{\Delta K,33,34}$; Supplementary Information, Table S1, Fig. S2) resulted in slightly shorter filopodia (10.0 ± 4.74 μm, n = 64; Fig. 5f) than co-expression with myosin IIIa$^{\Delta K}$. Using COS-7 cell co-expression and GST pulldown assays, we confirmed that the upstream portion of 3THDI (3THDI$^{\Delta 33}$, Supplementary Information, Fig. S4) binds to espin 1. The 3THDII of myosin IIIa has

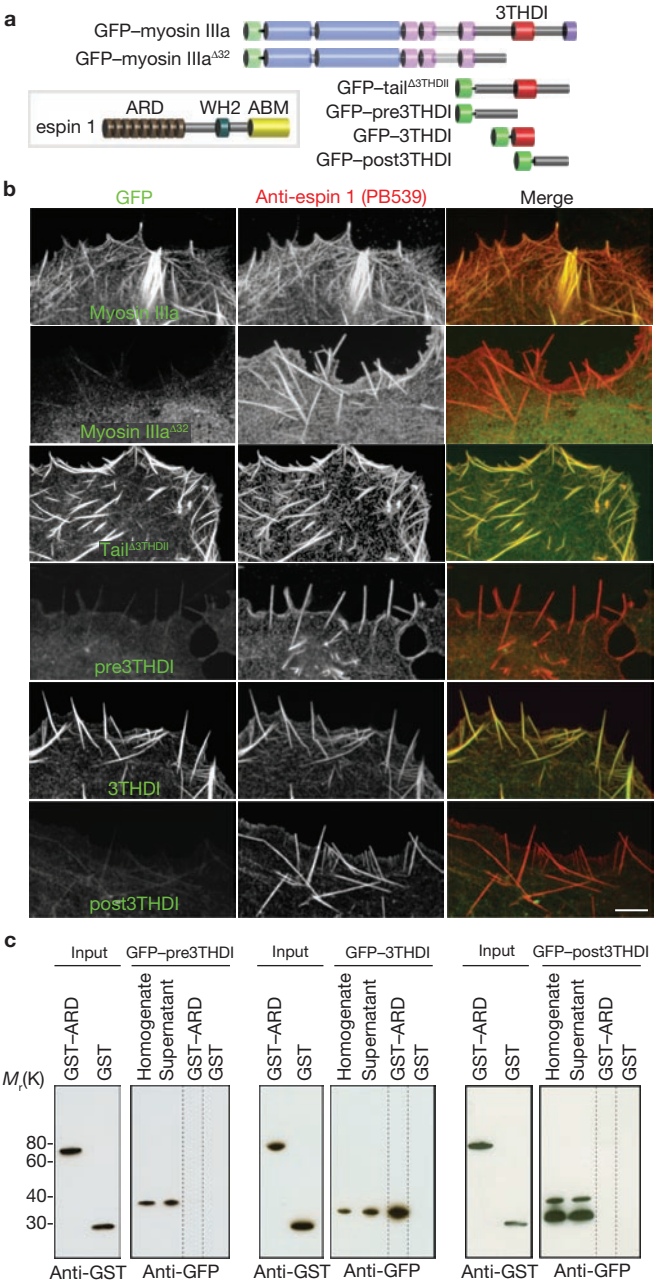

Figure 4 Myosin IIIa interacts with espin 1 through its 3THDI domain. (**a**) Schematic representation of the espin 1 and myosin IIIa constructs analysed in this figure. ABM, actin binding module; WH2, Wiskott-Aldrich homology domain 2; GFP–myosin IIIa$^{\Delta 32}$, myosin IIIa lacking exon 32 which causes a frame shift rendering the protein without the 3THDI and 3THDII domains. (**b**) Co-expression of untagged espin 1 shows that GFP–myosin IIIa, GFP–tail$^{\Delta 3THDII}$, and GFP–3THDI (green) colocalize with espin 1 (red) along actin filament bundles. In contrast, GFP–myosin IIIa$^{\Delta 32}$, GFP–pre-, and post3THDI are dispersed in the cytoplasm, despite the presence of espin 1 bundles. Scale bar, 5 μm. (**c**) Western blots of GST pulldowns confirm that the 3THDI region of myosin IIIa is necessary and sufficient for binding to espin 1-ARD, as pre3THDI and post3THDI show no binding to GST–ARD. Precipitates were detected using anti-GST and anti-GFP antibodies.

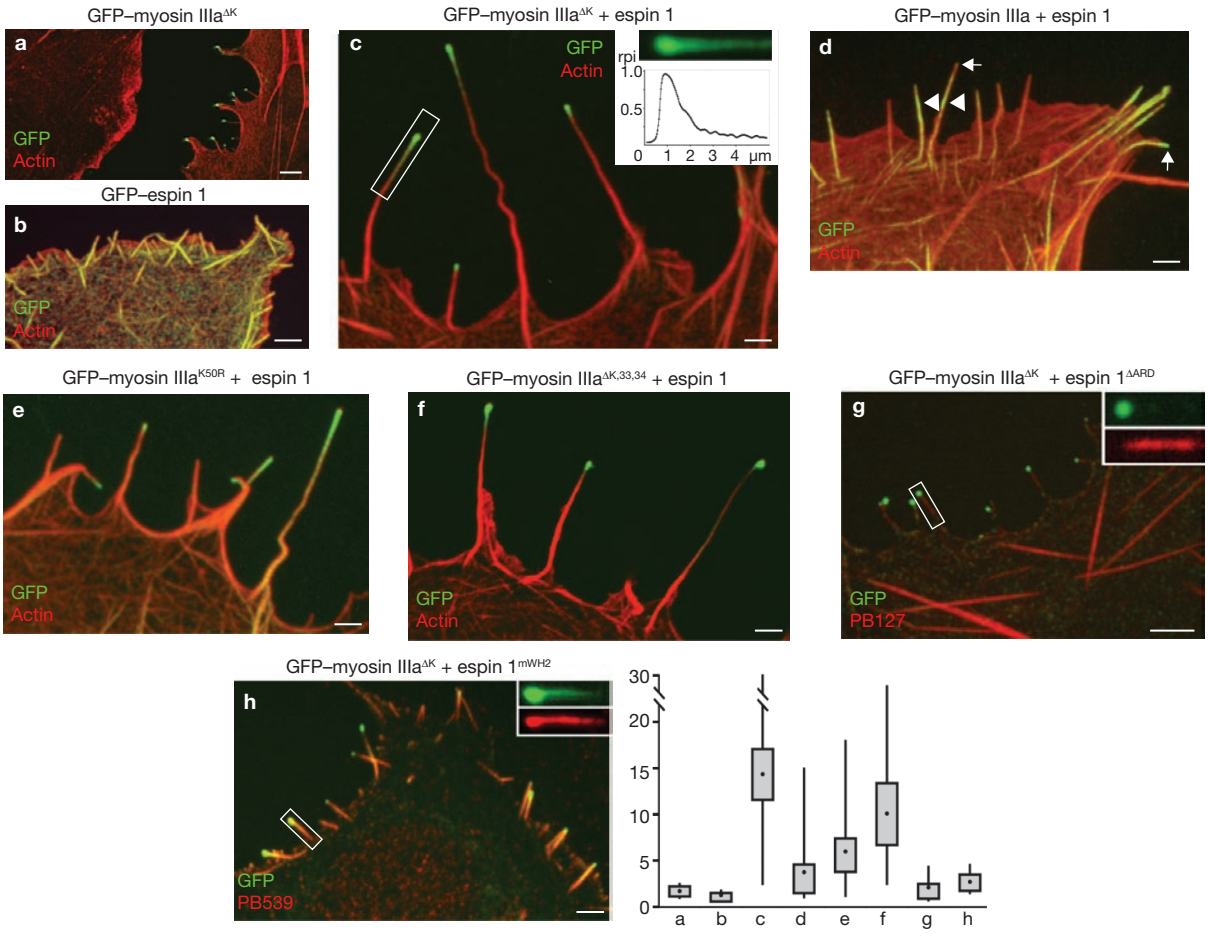

Figure 5 Myosin IIIa and espin 1 synergistically elongate filopodia in COS-7 cells through espin 1 WH2 activity. (**a**–**c**) Overexpression of either GFP–myosin IIIa$^{\Delta K}$ (**a**) or GFP–espin 1 (**b**) resulted in formation of short filopodia (mean lengths = 1.7 ± 0.83 μm and 1.3 ± 0.28 μm, respectively). In contrast, co-expression of GFP–myosin IIIa$^{\Delta K}$ (green) and espin 1 (**c**) had a synergistic effect that generated extremely long filopodia (14.3 ± 9.1 μm). F-actin (red) was visualized using Alexa 568-phalloidin. Graph (inset) of the relative pixel intensity (rpi) of the GFP–myosin IIIa$^{\Delta K}$ distribution in the single filopodium indicated by the rectangle in **c** shows the characteristic tip-to-base decaying gradient. (**d**) Co-expression of full-length GFP–myosin IIIa and espin 1 produced a more limited tip localization of these proteins and elongation of filopodia (3.7 ± 3.2 μm) when compared with co-expression of GFP–myosin IIIa$^{\Delta K}$ and espin 1. (**e**) The enhanced elongation phenotype was restored to a limited extent (5.93 ± 3.10 μm) when COS-7 cells were co-transfected instead with GFP–myosin IIIa^{K50R} and espin 1. **(f)** The enhanced elongation phenotype was similar to **c** when the cell was co-transfected with GFP–myosin IIIa$^{\Delta K,33,34}$ and espin 1 (10.02 ± 4.7 μm). (**g**) Co-expression of GFP–myoIIIa$^{\Delta K}$ and espin 1 lacking ARD (espin 1$^{\Delta ARD}$, labelled with the pan espin antibody, red) failed to elongate filopodia (2.05 ± 1.8 μm) and to show tip localization of espin 1$^{\Delta ARD}$ (inset). **(h)** Co-expression of GFP–myosin IIIa$^{\Delta K}$ and espin 1 with a mutated WH2 domain (espin 1^{mWH2}, labelled with an anti-espin 1 antibody, red) failed to elongate filopodia (2.65 ± 1.5 μm) despite the fact that espin 1^{mWH2} localized to the tip and formed the tip-to-base gradient matching the distribution of the GFP–myoIIIa$^{\Delta K}$ (inset). Scale bars, 2.5 μm. Measurements of filopodia lengths for each of the combinations shown in the panels above are presented as box-plots; upper and lower whiskers represent the range, the top and bottom of the box represent the upper and lower 25th percentile, and the filled squares represent the mean values.

been shown previously to be an actin-binding site[18]. Previous studies reported that myosin IIIa lacking the 3THDII actin-binding domain does not localize to filopodia tips[7,18], but here we show that when co-expressed with espin 1, myosin IIIa goes to the tip and promotes filopodia elongation (Fig. 5f). It seems that the association with espin 1, which does have actin-binding sites, compensates for the missing actin-binding site in the myosin IIIa without the 3THDII domain.

Co-expression of espin 1 and myosin IIIa results in enhanced localization of espin 1 at filopodia tips (Supplementary Information, Fig. S5). When myosin IIIa$^{\Delta K}$ was co-expressed with espin 1 lacking the ARD domain, both espin tip localization and filopodia elongation were abolished (Fig. 5g). These results show that the actin crosslinking activity of espin 1 is not solely responsible for the enhanced elongation of filopodia or stereocilia observed in our experiments. We conclude that espin 1 promotes enhanced elongation of filopodia only when transported to the polymerization end of actin filaments by myosin IIIa. The finding that espin 1 elongates filopodia only when localized to the F-actin plus ends by myosin IIIa suggests that WH2-dependent polymerization activity is involved in elongation. We tested this hypothesis by substituting the first two of three highly conserved Leu residues of the espin 1 WH2 motif (L655A, L656A), which have been shown to be essential for its actin-monomer-binding activity[21,22]. In COS-7 cells co-transfected with the WH2-mutated espin 1 construct (espin 1^{mWH2}) and myosin IIIa$^{\Delta K}$ (Fig. 5h), the average length of filopodia (2.65 ± 1.50 μm, $n_c = 10$, $n_f = 75$) remained comparable to the protrusions induced by myosin IIIa$^{\Delta K}$ alone. The lack of enhanced elongation despite the colocalization of espin 1^{mWH2} and myosin IIIa$^{\Delta K}$ at the tips of filopodia (Fig. 5h) demonstrates that the WH2 motif is essential for the effect of espin 1 in elongation.

The steady-state distribution of myosin IIIa in a tip-to-base gradient is probably dynamically maintained. The length of myosin IIIa distribution should be inversely proportional to the net velocity of myosin towards the tip[23], which will be slower for faster treadmilling actin cores (that is, in longer stereocilia[9] and filopodia[24]). This prediction is also consistent with our observation that wild-type myosin IIIa, which has relatively low activity, has decreased tip localization in the filopodia, compared with the more active kinase mutant forms of myosin IIIa used in our experiments (Fig. 5). However, in stereocilia where the actin treadmilling is much slower, the wild-type myosin IIIa self-localizes effectively to the tip[7] (Fig. 2). Similarly, the observed steady-state tip-to-base gradient distribution of espin 1 is not compatible with a model where espin 1 passively diffuses and binds to myosin IIIa resident at the tip, as this would result in a homogenous distribution along the entire length of the stereocilia with no detectable concentration gradient at steady-state. The gradient distribution of espin 1 at steady-state is reminiscent of a myosin VI-driven gradient for the stereocilia membrane protein PTPRQ, and is best explained by a model that includes binding, directed transport and diffusion of myosins and their cargo[25]. A more detailed consideration of this dynamic process that also accounts for actin treadmilling and plus-end directed motors predicts a similar distribution, which can be several microns long for longer stereocilia[23]. Thus, we favour a model where myosin IIIa–espin 1 complexes are dynamically associated with the treadmilling actin core. This model suggests that espin 1 is transported to the tips of stereocilia by myosin IIIa, where it remains bound to the surface of the actin core for a period of time. Interestingly, abolishing or reducing myosin IIIa kinase activity enhances the affinity of myosin IIIa for actin, providing further evidence that the kinase domain has a role in regulating myosin IIIa motor kinetics and actin-binding properties[26,27]. While the myosin IIIa–espin 1 complex is tightly bound to actin, it travels back towards the base of the stereocilia along with the treadmilling actin core. In support of this model, live video imaging in transfected COS-7 cells shows fluorescent puncta of GFP–myosin IIIa$^{\Delta K}$ and mCherry–ARD (Supplementary Information, Movie 4) that move rearwards at rates matching the rates reported for actin treadmilling in filopodia (~0.5 μm min^{-1})[24]. We suggest that these puncta are stably bound to the surface of the treadmilling actin filament bundle.

Notably, the stereocilia tips are also the site of mechanoelectrical transduction (MET)[28], that the myosin IIIa developmental expression level is correlated with maturation of MET in stereocilia[17], and that myosin IIIa has been shown to transport components of the photoreceptor transduction machinery in *Drosophila*[29,30]. We cannot exclude the possibility that the localization and dynamics of the myosin IIIa–espin 1 complex are also affected by interactions with other proteins at the stereocilia tip. Furthermore, ankyrin repeats have been shown to be promiscuous binders of membrane proteins[31]. It is possible that the turnover and dynamic localization of the espin 1–myosin IIIa complex are influenced by interactions with components of the MET machinery, and vice-versa. □

METHODS

Antibodies. Affinity-purified polyclonal antibodies (PB538 and PB539) were developed in rabbits immunized with a synthetic peptide (Princeton Biomolecules) corresponding to the amino acid sequence (LDALPVHHAARSGKLHCLR) of the first ankyrin repeat of mouse espin 1. A similarly raised antibody specific for a region conserved in all isoforms of espin (pan-espin, PB127; ref. 8) and anti-myosin IIIa (PB638; ref. 7) antibodies have been previously described.

Immuofluorescence and microscopy. After CO_2 anaesthesia, rats, mice and guinea pigs were euthanized in accordance with National Institutes of Health (NIH) guidelines, and their temporal bones fixed by immersion in 4% paraformaldehyde in phosphate buffered saline (PBS; pH 7.4) for 2 h at room temperature. Sensory tissue was dissected in PBS, permeabilized with 0.5% Triton X-100 for 30 min and blocked overnight at 4 °C with 4% bovine serum albumin in PBS. Tissues were then incubated with primary antibody for 2 h, rinsed with PBS, stained with Alexa Fluor 488-conjugated secondary antibody (Molecular Probes) for 1 h, counterstained with Alexa Fluor 568 phalloidin (0.001 U μl^{-1}; Molecular Probes) and mounted using Prolong Antifade (Molecular Probes). Fluorescence confocal images were obtained with a Nikon microscope equipped with a ×100 1.45 numerical aperture (NA) objective and a spinning disk confocal unit (PerkinElmer).

Electron microscopy. Rat organ of Corti or vestibular tissues were either rapidly frozen by contact with a liquid nitrogen cooled metal block in a LifeCell (The Woodlands) freezing apparatus or fixed, glycerinated and plunge-frozen in Freon 22 cooled in liquid nitrogen before freeze-substitution in 1.5% uranyl acetate in absolute methanol at –90 °C. Freeze-substituted tissues were infiltrated with Lowicryl HM-20 resin (Electron Microscopy Sciences) at –45 °C, polymerized with UV light, thin-sectioned and labelled with immunogold. Samples were viewed and photographed with a Zeiss 922 electron microscope. As control for the immunogold labelling, we also used the antibody PB288, which is unrelated to espin or to myosin IIIa (Supplementary Information, Fig. 1d).

Expression plasmids. Espin 1 (NCBI accession number NM_031475) in pSPORT1 vector was obtained from imaGenes and PCR-cloned into pEGFP-C2 (Clontech) and pcDNA3.1(–) (Invitrogen) through *Eco*RI and *Kpn*I sites. The site-directed Leu to Ala mutations in the WH2 motif of espin 1 were generated using a GeneTailor site-directed mutagenesis kit (Invitrogen). The ARD between amino acid positions 16 and 363 was PCR-amplified using the mouse espin 1 template (NM_207687) and subcloned in-frame into the mCherry-C1 (Clontech) expression vector through *Xho*I and *Eco*RI sites, and pDEST 15 GST expression vector (Invitrogen) using the Gateway LR Clonase cloning method (Invitrogen). The GFP-tagged expression plasmids used were espin 1$^{\Delta ARD}$ (a gift from James Bartles, Northwestern University, Chicago IL), myosin X (a gift from Richard Cheney, UNC, Chapel Hill NC), myosin XVa (a gift from Thomas Friedman, NIDCD/NIH), as well as full-length and deletion constructs of myosin IIIa that were generated in our laboratories. Myosin IIIa 2IQ$^{\Delta K}$ constructs were generated as described previously[26,34]. Myosin IIIa 2IQ^{K50R} and myosin IIIa^{K50R} constructs were generated by performing site-directed mutagenesis on the myosin IIIa 2IQ and myosin IIIa full-length constructs, respectively. All expression plasmids were sequence verified. Further details about the clones used are available in Supplementary Information, Table S1 and Fig. S3.

Cultures and transfection of COS-7 cells. COS-7 (ATCC) cells were plated on coverslips and maintained at 37 °C in DMEM with 10% FBS. Cultures were transfected using GeneJuice transfect reagent (Novagen) and incubated for 24 h. Time-lapse videos of live cells were acquired at the maximum nominal laser power and camera gain allowed by the confocal microscope. Samples were also fixed for 20 min in 4% paraformaldehyde in PBS, permeabilized for 30 min in 0.5% Triton X-100 in PBS, and counterstained or processed for immunofluorescence as described above.

Culture and transfection of rat inner ear tissue. Organ of Corti and vestibular tissues were dissected from postnatal day 0–4 rats and attached to coverslips previously coated with Cell-Tak (150 μg μl^{-1}; BD Biosciences). Cultures were maintained in DMEM/F12 (Invitrogen) with 5–7% fetal bovine serum (FBS) and ampicillin (1.5 μg ml^{-1}; Sigma) and kept at 37 °C and 5% CO_2. For transfections, 50 μg of DNA was precipitated onto 25 mg of 1 μm gold particles and loaded into the Helios Gene Gun cartridges (BioRad). Tissue explants were transfected with the gene gun set at 95 psi of helium and maintained in culture for 18–48 h. Samples were fixed and counterstained for confocal microscope viewing as described above. The efficiency of transfection ranged from 0–9 hair cells per explant.

Image analysis. Image analysis was performed with ImageJ software (NIH). To estimate the relative increase in stereocilia length, we compared the heights of the tallest row of well-preserved stereocilia of cochlear and vestibular hair cells transfected

(H_t) with the average height of all their respective neighbouring (usually between 3–5) non-transfected cells (H_{nt}) within the field of view of our camera/confocal setup (30 × 45 μm). The average ratio of stereocilia length was calculated as $1 = \frac{H_T}{H_{NT}}$. ANOVA was performed using MATLAB (Mathworks). Cross-correlation analysis for the intensity plot in Fig. 3 was performed using Microsoft Excel.

Western blotting. 100-mm dishes of transfected semi-confluent COS-7 cells were rinsed in PBS and scraped in 160 μl of lysis buffer: PBS, 1% Triton-X, 5 mM DTT, 1 mM Pefabloc, 5 μg ml^{-1} pepstatin A, 5 μg ml^{-1} leupeptin, 2 mM EDTA, 0.2 mM PMSF and 1% mammalian protease inhibitor cocktail (Sigma). After addition of 1× loading sample buffer and dithiothreitol (Invitrogen), samples were boiled and 10 μl of lysates were loaded in 4–12% Bis-Tris minigel (Invitrogen). Western blots were incubated overnight at 4 °C with 4 μg ml^{-1} of the primary antibody. Horseradish peroxidase-conjugated goat anti-rabbit antibodies (Santa Cruz) and ECL chemiluminescence system (Amersham Biosciences) were used for detection.

GST pulldown assays. Protein expressions of glutathione S-transferase (GST) alone or fused to ARD (GST–ARD) were optimized under L-arabinose induction in BL21-AI bacteria (Invitrogen). GST proteins were purified from bacterial extracts using glutathione–Sepharose 4B beads according to the manufacturer's instructions (Amersham Biosciences). GFP–myosin IIIa$^{\Delta K}$, – pre3THDI, –3THDI and –post3THDI proteins were extracted from 24-h COS-7 transfectants by brief sonication and 20-min ultracentrifugation at 145,000*g* in ice-cold lysis buffer (1% Triton X-100, 5 mM DTT, 150 mM NaCl, 50 mM Tris pH 7.4, 2 mM EDTA, 3 mM Pefabloc SC, 1× Pefabloc (Roche) and 1× mammalian protease inhibitor cocktail (Sigma)). To test for myosin IIIa interactions, the same amount of GST–ARD or GST alone was bound to 4B beads for 1 h at 4 °C followed by incubation with the GFP-tagged myosin IIIa fragment in CLB for 2 h. The beads were then washed four times with lysis buffer. Bound proteins were separated by electrophoresis on NuPAGE Bis-Tris 4-12% gels (Invitrogen) and analysed by western blotting using rabbit polyclonal anti-GFP and anti-GST antibodies (Invitrogen).

ATPase assays. The steady-state actin-activated ATPase activity of baculovirus-expressed myosin IIIa 2IQ^{K50R} and wild-type were assessed in an NADH-coupled assay[26,32]. ATPase activity of fully phosphorylated myosin IIIa was compared with unphosphorylated myosin IIIa after a 60-min incubation at room temperature in the presence and absence of 200 μM ATP, respectively. The kinase activity of the myosin IIIa 2IQ constructs was assayed using ^{32}P-ATP or western blotting with anti-phosphothreonine antibodies[26,32].

Note: Supplementary Information is available on the Nature Cell Biology website.

ACKNOWLEDGEMENTS

We thank Chi W. Pak for discussions and for the suggestion of mutations in the WH2 motif, Mark Schneider and Saeeda Latham for initial help with experiments and for discussions related to this work, Martin Horak for advice on cloning procedures, and Ronald Petralia for comments on the manuscript. This work was supported by NIDCD, DIR, NIH and in part by NIH grants to A.C.D. (no. EY003575) and to C.M.Y. (no. EY016419).

AUTHOR CONTRIBUTIONS

R.C.M. designed probes and experiments, performed the GST pulldowns, cell culture, immunocytochemistry and transfections; F.T.S. performed the dissections, cell and organotypic cultures, immunohistochemistry, transfections and confocal imaging; G.W.D. and A.C.D. designed probes, performed transfections and contributed to the experimental design; U.M. performed image and statistical analyses; A.D.S. characterized antibody and DNA probes; C.M.Y. and J.E.M. generated myosin IIIa kinase dead cDNA, purified and performed kinase and motor activity assays; B.K. performed electron microscopy, designed experiments and analysed the results together with all the other authors. All authors discussed and helped to prepare the manuscript.

COMPETING FINANCIAL INTERESTS

The authors declare no competing financial interests.

Published online at http://www.nature.com/naturecellbiology/
Reprints and permissions information is available online at http://npg.nature.com/reprintsandpermissions/

1. Walsh, T. *et al.* From flies' eyes to our ears: mutations in a human class III myosin cause progressive non-syndromic hearing loss DFNB30. *Proc. Natl Acad. Sci. USA* 99, 7518–7523 (2002).
2. Komaba, S., Inoue, A., Maruta, S., Hosoya, H. & Ikebe, M. Determination of human myosin III as a motor protein having a protein kinase activity. *J. Biol. Chem.* 278, 21352–21360 (2003).
3. Zheng, L. *et al.* The deaf jerker mouse has a mutation in the gene encoding the espin actin-bundling proteins of hair cell stereocilia and lacks espins. *Cell* 102, 377–385 (2000).
4. Donaudy, F. *et al.* Espin gene (ESPN) mutations associated with autosomal dominant hearing loss cause defects in microvillar elongation or organisation. *J. Med. Genet.* 43, 157–161 (2006).
5. Naz, S. *et al.* Mutations of ESPN cause autosomal recessive deafness and vestibular dysfunction. *J. Med. Genet.* 41, 591–595 (2004).
6. Sekerkova, G., Zheng, L., Loomis, P. A., Mugnaini, E. & Bartles, J. R. Espins and the actin cytoskeleton of hair cell stereocilia and sensory cell microvilli. *Cell. Mol. Life Sci.* 63, 2329–2341 (2006).
7. Schneider, M. E. *et al.* A new compartment at stereocilia tips defined by spatial and temporal patterns of myosin IIIa expression. *J. Neurosci.* 26, 10243–10252 (2006).
8. Rzadzinska, A., Schneider, M., Noben-Trauth, K., Bartles, J. R. & Kachar, B. Balanced levels of Espin are critical for stereociliary growth and length maintenance. *Cell. Motil. Cytoskeleton* 62, 157–165 (2005).
9. Rzadzinska, A. K., Schneider, M. E., Davies, C., Riordan, G. P. & Kachar, B. An actin molecular treadmill and myosins maintain stereocilia functional architecture and self-renewal. *J. Cell Biol.* 164, 887–897 (2004).
10. Lin, H. W., Schneider, M. E. & Kachar, B. When size matters: the dynamic regulation of stereocilia lengths. *Curr. Opin. Cell Biol.* 17, 55–61 (2005).
11. Schneider, M. E., Belyantseva, I. A., Azevedo, R. B. & Kachar, B. Rapid renewal of auditory hair bundles. *Nature* 418, 837–838 (2002).
12. Manor, U. & Kachar, B. Dynamic length regulation of sensory stereocilia. *Semin. Cell Dev. Biol.* 19, 502–510 (2008).
13. Belyantseva, I. A. *et al.* Myosin-XVa is required for tip localization of whirlin and differential elongation of hair-cell stereocilia. *Nature Cell Biol.* 7, 148–156 (2005).
14. Prosser, H. M., Rzadzinska, A. K., Steel, K. P. & Bradley, A. Mosaic complementation demonstrates a regulatory role for myosin VIIa in actin dynamics of stereocilia. *Mol. Cell Biol.* 28, 1702–1712 (2008).
15. Tokuo, H., Mabuchi, K. & Ikebe, M. The motor activity of myosin-X promotes actin fiber convergence at the cell periphery to initiate filopodia formation. *J. Cell Biol.* 179, 229–238 (2007).
16. Tokuo, H. & Ikebe, M. Myosin X transports Mena/VASP to the tip of filopodia. *Biochem. Biophys. Res. Commun.* 319, 214–220 (2004).
17. Waguespack, J., Salles, F. T., Kachar, B. & Ricci, A. J. Stepwise morphological and functional maturation of mechanotransduction in rat outer hair cells. *J. Neurosci.* 27, 13890–13902 (2007).
18. Les Erickson, F., Corsa, A. C., Dose, A. C. & Burnside, B. Localization of a class III myosin to filopodia tips in transfected HeLa cells requires an actin-binding site in its tail domain. *Mol. Biol. Cell* 14, 4173–4180 (2003).
19. Bohil, A. B., Robertson, B. W. & Cheney, R. E. Myosin-X is a molecular motor that functions in filopodia formation. *Proc. Natl Acad. Sci. USA* 103, 12411–12416 (2006).
20. Dose, A. C. *et al.* Myo3A, one of two class III myosin genes expressed in vertebrate retina, is localized to the calycal processes of rod and cone photoreceptors and is expressed in the sacculus. *Mol. Biol. Cell* 14, 1058–1073 (2003).
21. Quinlan, M. E., Heuser, J. E., Kerkhoff, E. & Mullins, R. D. *Drosophila* Spire is an actin nucleation factor. *Nature* 433, 382–388 (2005).
22. Loomis, P. A. *et al.* Targeted wild-type and jerker espins reveal a novel, WH2-domain-dependent way to make actin bundles in cells. *J. Cell Sci.* 119, 1655–1665 (2006).
23. Naoz, M., Manor, U., Sakaguchi, H., Kachar, B. & Gov, N. Protein localization by actin treadmilling and molecular motors regulates stereocilia shape and treadmilling rate. *Biophys. J.* (2008).
24. Mallavarapu, A. & Mitchison, T. Regulated actin cytoskeleton assembly at filopodium tips controls their extension and retraction. *J. Cell Biol.* 146, 1097–1106 (1999).
25. Sakaguchi, H. *et al.* Dynamic compartmentalization of protein tyrosine phosphatase receptor Q. at the proximal end of stereocilia: Implication of myosin VI-based transport. *Cell. Motil. Cytoskeleton* (2008).
26. Dose, A. C. *et al.* The kinase domain alters the kinetic properties of the myosin IIIA motor. *Biochemistry* 47, 2485–2496 (2008).
27. Kambara, T., Komaba, S. & Ikebe, M. Human myosin III is a motor having an extremely high affinity for actin. *J. Biol. Chem.* 281, 37291–37301 (2006).
28. Ricci, A. J., Kachar, B., Gale, J. & Van Netten, S. M. Mechano-electrical transduction: new insights into old ideas. *J. Membr. Biol.* 209, 71–88 (2006).
29. Porter, J. A., Yu, M., Doberstein, S. K., Pollard, T. D. & Montell, C. Dependence of calmodulin localization in the retina on the NINAC unconventional myosin. *Science* 262, 1038–1042 (1993).
30. Wes, P. D. *et al.* Termination of phototransduction requires binding of the NINAC myosin III and the PDZ protein INAD. *Nature Neurosci.* 2, 447–453 (1999).
31. Mosavi, L. K., Cammett, T. J., Desrosiers, D. C. & Peng, Z. Y. The ankyrin repeat as molecular architecture for protein recognition. *Protein Sci.* 13, 1435–1448 (2004).
32. Dose, A. C., Ananthanarayanan, S., Moore, J. E., Burnside, B. & Yengo, C. M. Kinetic mechanism of human myosin IIIA. *J. Biol. Chem.* 282, 216–231 (2007).

nature cell biology

DOI: 10.1038/ncb1851

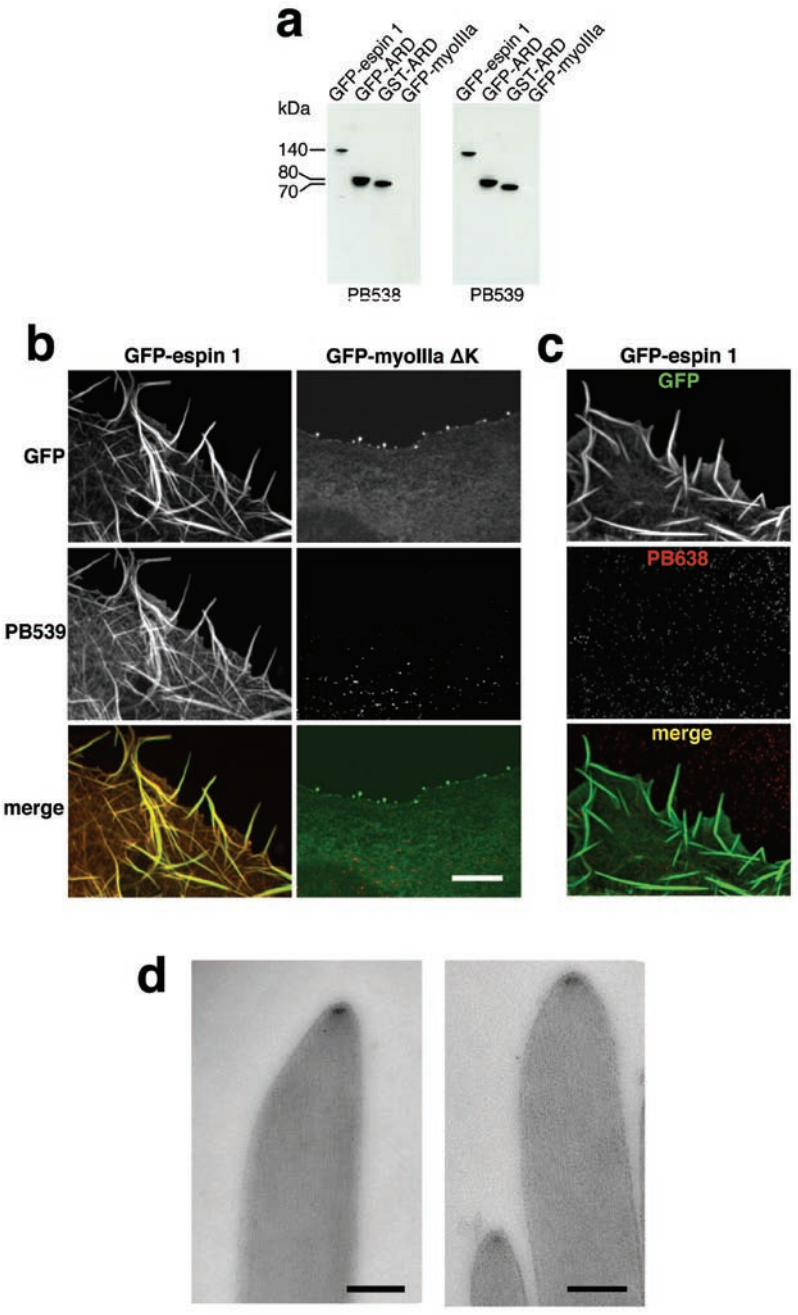

Figure S1 Specificity of the antibodies generated against the ARD of espin 1. (**a**) Immunoblots of lysates from COS-7 cells transfected with GFP-espin 1, GFP-ARD, and GFP-myoIIIa ΔK as well as lysates from bacteria expressing GST-ARD show that both PB538 and PB539 specifically recognize the ARD of espin 1. (**b**) GFP-espin 1 (left column) overexpressed in COS-7 cells is recognized by PB539. The same antibody shows no labeling in COS-7 cells with overexpressing GFP-myoIIIa ΔK only (right column). (**c**) In the negative control, our myosin IIIa specific antibody (PB638) fails to recognize GFP-espin 1 in COS-7 cells. GFP constructs are in green and Alexa Fluor 568-conjugated secondary antibody is red. Scale bar is 5 μm. (**d**) Control experiments for the post embedding immunogold labeling in directly frozen freeze-substituted adult rat cochlear hair cells shows no gold labeling at the tip of stereocilia when using the PB288 antibody, unrelated to espin 1 and myosin IIIa. Scale bars, 200 nm.

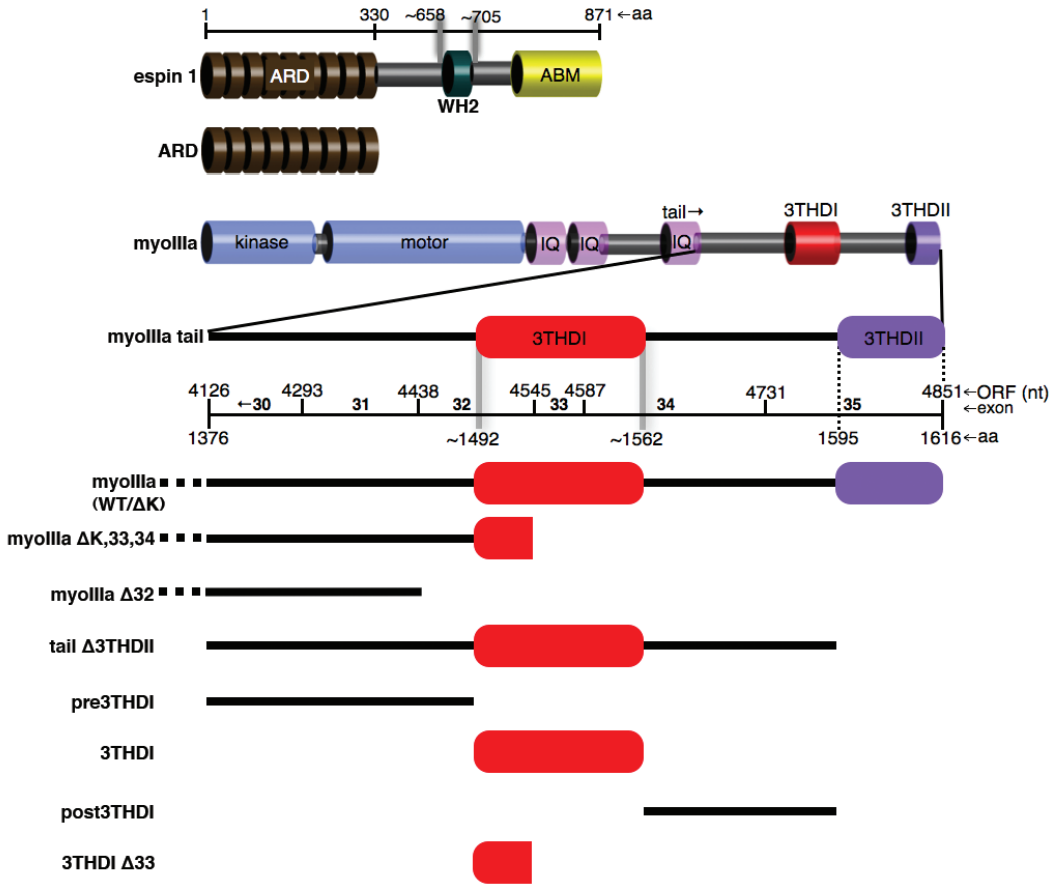

Figure S2 Schematic map of wild-type and deletion constructs. Only the myosin IIIa coding regions are shown. Full-length espin 1 is 871 amino acid-long in mouse and 854 amino acid-long in human (mouse espin 1 is illustrated here). The tail domain of myoIIIa encompasses 3THDI, 3THDII, and the third IQ domain, however; only 3THDI and 3THDII were considered in this study. Myosin IIIa Δ32 lacks exon 32, which causes a frame shift eliminating 3THDI and 3THDII, and introduces 26 new amino acids. Myosin IIIa Δ33,34 lacks exons 33 and 34, which causes a frame shift approximately one third of the way through 3THDI and therefore eliminates the rest of 3THDI and 3THDII, and introduces 72 new amino acids.

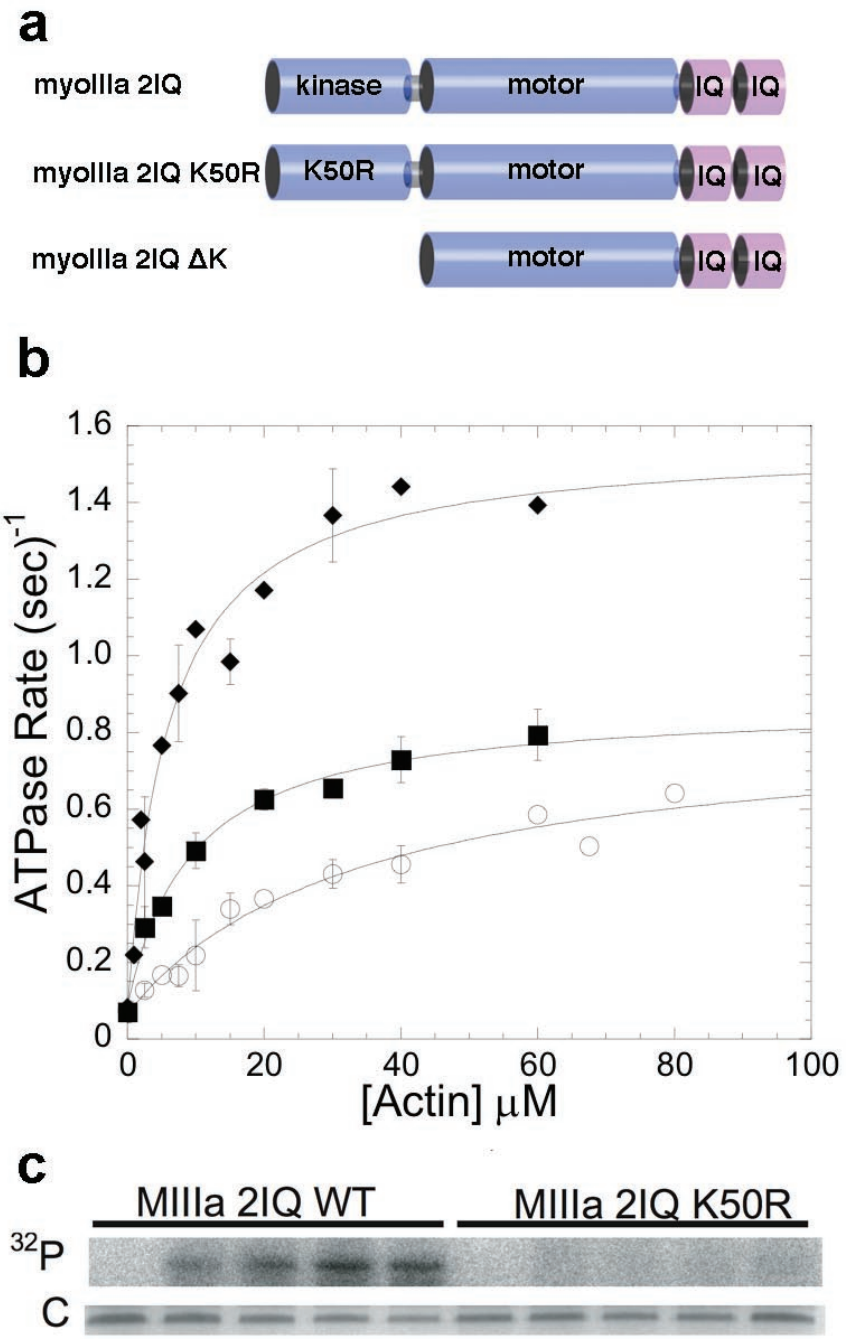

Figure S3 Actin-activated ATPase activity of myosin IIIa 2IQ constructs. **a**) A diagram of the myosin IIIa 2IQ constructs examined. **b**) The results for myosin IIIa 2IQ K50R (squares) are compared to that of myosin IIIa 2IQ wild-type [37] (open circles) and myosin IIIa 2IQ ΔKinase[28] (diamonds). The steady-state ATPase rate of 0.1 μM myosin was measured using the NADH coupled assay in the presence of 1 mM ATP and a range of actin concentrations. The error bars represent the standard deviation from the mean and include data from 3-4 protein preparations. The enzymatic parameters determined from the fits to the data are summarized in the Table S2. Full phosphorylation of myosin IIIa 2IQ results in a ~ 40% reduction in ATPase activity compared to unphosphorylated myosin IIIa 2IQ, in the presence of 20 μM actin (data not shown). A previous study reported the kinetic mechanisms of the myosin IIIa 2IQ ΔKinase[28] and myosin IIIa 2IQ WT[37] constructs, which demonstrated the specific steps in motor ATPase cycle that are altered by the presence of the kinase domain. **c**) The kinase activity of 1 μM myosin IIIa 2IQ WT was monitored by ^{32}P incorporation (200 μM [^{32}P]ATP) over a 60 minute period (lanes 1-5 are 0, 5, 15, 30, and 60 minute time points, respectively). The results are compared to myosin IIIa 2IQ K50R that demonstrated little or no kinase activity under identical conditions (lanes 6-10 are 0, 5, 15, 30, and 60 minute time points, respectively). The top panel, labeled ^{32}P, is the phosphorimage demonstrating the degree of ^{32}P incorporation while the bottom panel, labeled C, is the same gel comassie stained to demonstrate that the total protein concentration in each lane is similar.

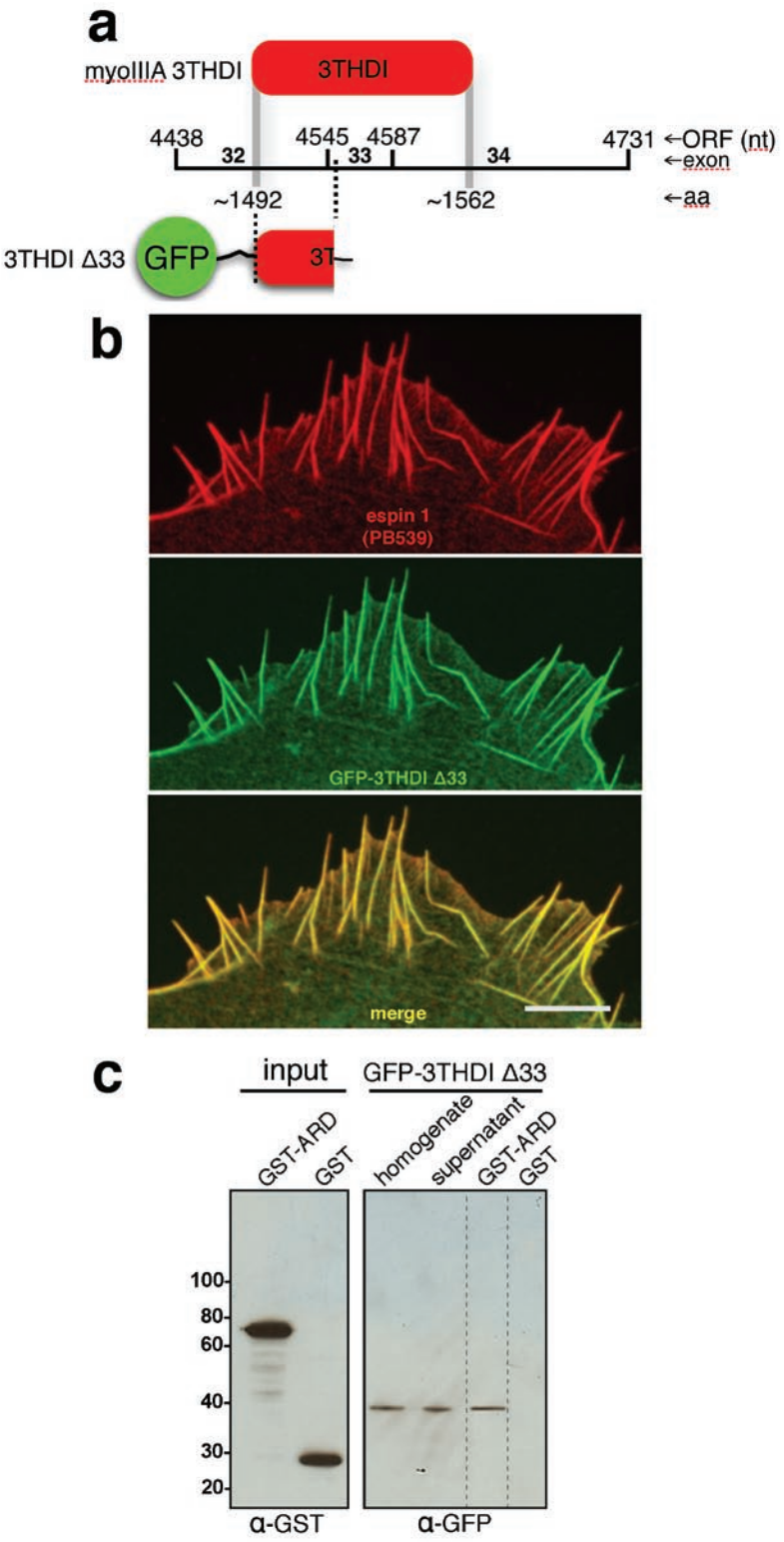

Figure S4 The first 24 amino acids of the 3THDI domain are sufficient for binding espin 1. (**a**) The mapping of the GFP-3THDI Δ33 fusion protein is illustrated. (**b**) GFP-3THDI Δ33 (green) colocalizes with espin 1 (red, labeled with PB539). PB539 (red) is labeled with Alexa Fluor 568-conjugated secondary antibody. Scale bar is 5 μm. (**c**) GST pull-down shows that GFP-3THDI Δ33 interacts with espin 1 ARD but not with GST.

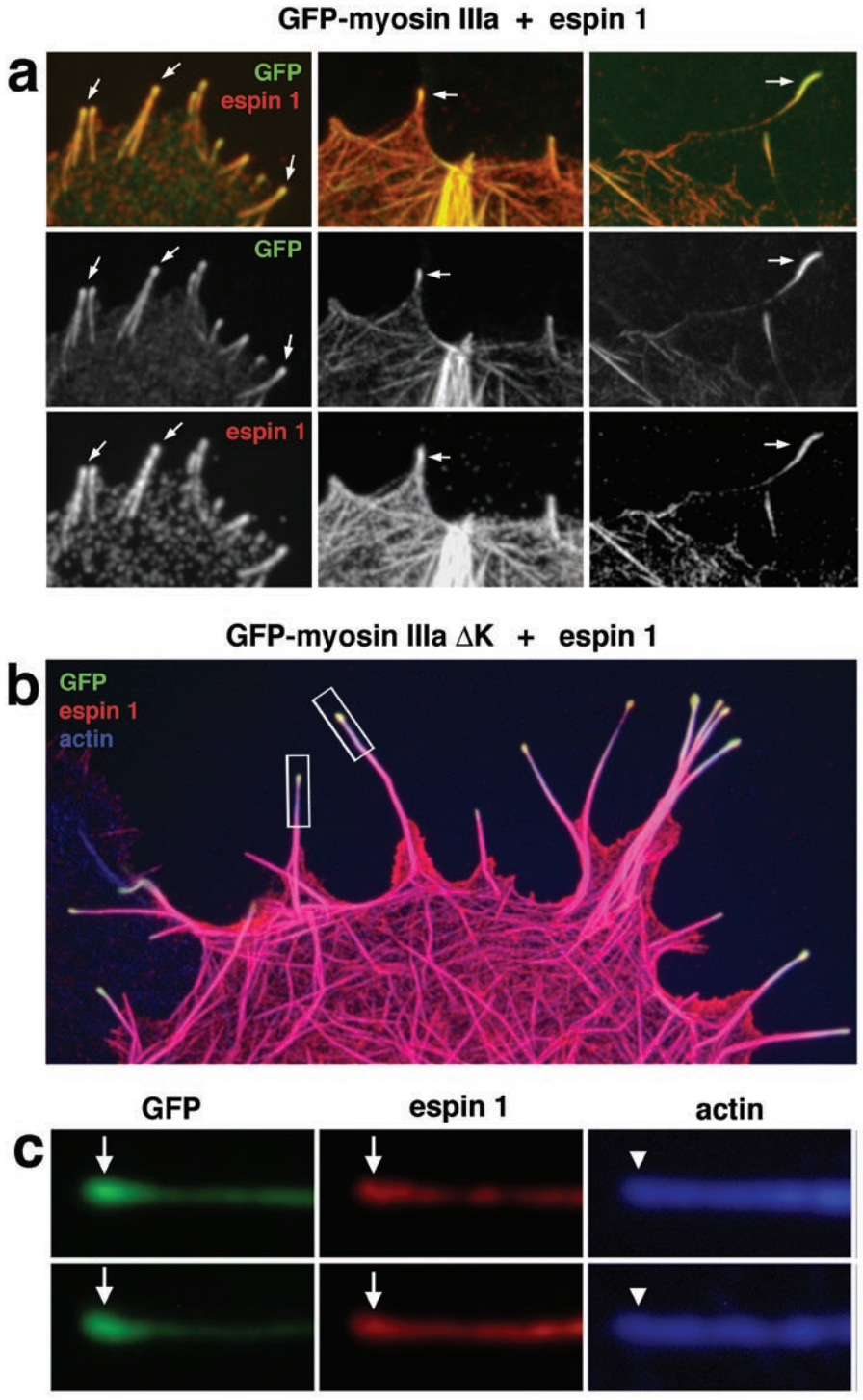

Figure S5 Co-localization of myosin IIIa and espin 1 at filopodia tips. (**a**) Close up views of COS-7 cells show that espin 1 (red) colocalizes with GFP-myoIIIa ΔK (green) at the filopodia tips when these two proteins are coexpressed in COS-7 cells. (**b**) Espin 1 (red) colocalizes with GFP-myoIIIa ΔK (green) at the filopodia tips (actin is labeled Alexa fluor 647 shown in blue) when these two proteins are coexpressed in COS-7 cells. (**c**) Close up views of the regions outlined by rectangles in (**b**) show the increased concentration of GFP-myosin IIIa ΔK (arrows, green) and espin 1 (arrows, red) but not actin (arrowheads, blue) at the filopodia tips. Bars = 3μm

Supplementary movie legends

Movie S1 Time-lapse imaging of the simultaneous expression of GFP-myosin IIIaΔK (top), mCherry-ARD (middle) in live COS-7 cells, and images merged (bottom). GFP-myosin IIIaΔK induces extension of filopodia and transports mCherry-ARD, accumulating at the tips of the actin protrusions. Cell was imaged 24 h after transfection. Video acquisition was performed for ten minutes with exposure times of 7.9 seconds for each frame (alternating 3.9 seconds for each of the green and red color channel).

Movie S2 GFP-myosin IIIa ΔK (green) and mCherry-ARD (red) co-expressed in COS-7 cells accumulate in a tip-to-base gradient in the resulting filopodia, while maintaining a dynamic bidirectional intra-filopodial observed as fluorescence puncta moving towards and away the filopodia tips. The colocalization of the moving puncta was demonstrated by the comparison of the plots of pixel intensity profiles for the green and the red channels in individual frames and the cross correlation analysis shown in figure 3C. Cell was imaged 24 h after transfection. Video acquisition was performed with exposure times of 4.2 seconds for each frame (alternating 2 seconds for each of the green and red color channel).

Movie S3 GFP-myosin IIIa ΔK (green) and mCherry-ARD (red) co-expressed in COS-7 cells accumulate in a tip-to-base gradient in the resulting filopodia, while maintaining a dynamic bidirectional intra-filopodial observed as fluorescence puncta moving towards and away the filopodia tips. Cell was imaged 24 h after transfection. Video acquisition was performed with exposure times of ~4 seconds for each frame (alternating exposure times of 1.5 seconds for the green channel and 2.3 seconds for the red channel). The total duration of the recoding was 5 min.

Movie S4 GFP-myosin IIIa ΔK (green) and mCherry-ARD (red) co-expressed in COS-7 cells accumulate in a tip-to-base gradient in the resulting filopodia, while maintaining dynamic intra-filopodial movements. Cell was imaged 24 h after transfection. Video acquisition was performed with exposure times of 7.9 seconds for each frame (alternating 3.9 seconds for each of the green and red color channel). Because of the longer exposure time than in the stream acquisition shown in **Video S2** this movie highlights the slower moving fluorescence puncta, which were estimated to be moving at ~0.5 μm/min in the retrograde direction.

Table S1. Novel clones and associated primers used in this study

DNA construct (aa)	Species (accession no.)	Vector	Forward primer	Reverse primer
GFP-myoIIIa Δ32 (1-1505)	human (AY101367)	pEGFP-C1	5′-GCTAGGATCCCACCA TGTTTCCATTAATTGGAAA AACAATCATC	5’-GTCTGCGGCCGCGTGCCTGC TGGTGCCAGCCCC
GFP-myoIIIa ΔK,33,34 (340-1587)			5’-GCTAGGATCCGTAGAT GATTTAGCAACCCTAGA AGTTTTGGATG	5’-GTCTGCGGCCGCGTGCCTG CTGGTGCCAGCCCC
GFP-myoIIIa K50R (1-1616)			5’-GCTAGGATCCCACCAT GTTTCCATTAATTGGAA AAACAATCATC	5’-GTCTGCGGCCGCGGACTGC TGGACGAGGCGCCG
GFP-tailΔ3THDII (1376-1594)			5′-CGTAGGATCCGCATC AGAGGATTGTCACAACAC CAACAGAAGTAGC	5′-GAGAGAGAGCCAGCAGC CACCCCCTACTAAGCGGCCGC ATCG
GFP-pre3THDI (1376-1491)			5′-CGTAGGATCCGCAT CAGAGGATTGTCACAA CACCAACAGAAGTAGC	5′-CTCAGGTGTCTGTAAAG GAGAGGAGCCAAAAATAT TGAGAGCGGCCGCATCG
GFP-3THDI (1492-1561)			5′-CGTAGGATCCCCCC CAAGACGACCCCGGA AACCCAAAAC	5′-CGATGCGGCCGCTCTTC GTTCTCTTAAACTAGGGC TATGTTCCTTTGGTCCAG
GFP-post3THDI (1562-1595)			5′-CGTAGGATCCCCAC AGCAAGAACTCCAGA ATCAATGTATTAAGGC TAATG	5′-GAGAGAGAGCCAGCAGC CACCCCCTACTAAGCGGCC GCATCG
GFP-3THDI Δ33 (1492-1525)		pcDNA 6.2/N-EmGFP-DEST	5′-CGTAGGATCCCCCC CAAGACGACCCCGGA AACCCAAAAC	5′-CGCTGGTCTTCGTTT TTCTTCTTG
myoIIIa K50R 2IQ (1-1143)		pEGFP-C1	5’-GCTAGGATCCCACCAT GTTTCCATTAATTGGAA AAACAATCATC	5’-GCTACGCCGGCGAATGAA TTCCTGATCAGAAGTTTGAA TGGTTGTTACTGCTGTG
V5-3THDI (1492-1553)	mouse (AY101368)	pcDNA/ nV5-DEST	5′-CCTCCAAGACGACC TCGGAAA	5′-TTATTTCCATTCTCTTGC ATTAGAGCT
mCherry-ARD (16-363)	mouse (NM_207687)	pmCherry-C1	5′-GACGTGCTGAGGTC CCTGC	5′-TTAGACCGACATGGTGG TGTTGG
GST-ARD		pDEST^{TM}15		
GFP-ARD		pcDNA 6.2/N-EmGFP-DEST		

Table S2. Steady-state motor ATPase parameters of the myosin IIIa 2IQ constructs.

Motor ATPase Parameters	MIIIa 2IQ	MIIIa 2IQ ΔK	MIIIa 2IQ K50R
[a]V_0 $(sec)^{-1}$	0.07 ± 0.03	0.08 ± 0.02	0.07 ± 0.05
[b]k_{cat} $(sec)^{-1}$	0.77 ± 0.08	1.5 ± 0.1	0.76 ± 0.08
[c]K_{ATPase} (μM)	34 ± 11	6.0 ± 1.4	11.9 ± 3.7

[a]Steady-state ATPase activity in the absence of actin measured with the NADH coupled assay.
[b]Maximum rate of actin-activated ATPase measured with the NADH coupled assay. The values for K_{ATPase} and k_{cat} were determined from the fit of the data in Figure S3 to the equation: $(V_0 + (k_{cat}\,[actin]) / (K_{ATPase} + [actin]))$.
[c]Actin concentration at which the actin-activated ATPase rate is one-half maximal from the NADH assay.